Catal Lett (2007) 119:199–208
DOI 10.1007/s10562-007-9229-z

Mesoporous Au/TiO_2 Catalysts for Low Temperature CO Oxidation

Y. Denkwitz · J. Geserick · U. Hörmann · V. Plzak · U. Kaiser · N. Hüsing · R. J. Behm

Received: 2 July 2007 / Accepted: 20 July 2007 / Published online: 4 August 2007

Abstract The activity and stability of structurally well defined mesoporous Au/TiO_2 catalysts with different support morphologies and pore sizes for low temperature CO oxidation was investigated by kinetic measurements and in-situ IR spectroscopy. The resulting catalysts with Au particle sizes of $\sim$3 nm exhibit a high activity for CO oxidation, similar to or exceeding that of highly active standard Au/TiO_2 catalysts with similar size Au nanoparticles and loading, and a significantly lower tendency for deactivation. Possible reasons for the improved performance of these catalysts are discussed.

Keywords Mesoporous catalysts · Activity · Deactivation · Au/TiO_2 · CO oxidation

1 Introduction

Oxide supported Au/MeO_x catalysts, in particular Au/TiO_2 catalysts, have been shown to be highly active for various oxidation and reduction reactions already at low temperatures [1–3], the most prominent one being the CO oxidation reaction [1, 4–8]. Mostly these catalysts are prepared by deposition-precipitation or impregnation procedures, using commercial titania such as P25 (Degussa AG) as support material [5, 9–13]. These support materials, which mostly consist of non porous primary particles, have rather low surface areas, and one might envision that the catalytic properties may be further enhanced by using higher surface area support materials, e.g., by stabilizing smaller Au nanoparticles. Such surface area effects were observed, e.g., for the water gas shift reaction [14]. Particularly interesting would be mesoporous oxide supports with pores in the few nanometer range, where the pores are large enough to allow unhindered access of the reactants to the Au particles by facile pore diffusion, and on the other hand small enough to stabilize the Au nanoparticles and possibly enhance the reactivity by an increased, accessible interface region between support and Au particles. The latter one results when support and Au particle contact at more than one region [15]. It was indeed reported recently that Au catalysts based on mesoporous aluminosilicates, on titania doped mesoporous SiO_2 or on a pure TiO_2 aerogel exhibit a high activity for CO oxidation [16–20], higher than that of Au/SiO_2 and Au/TiO_2 catalysts, respectively, on commercial supports. The Au surface normalized rates are, however, only half of those obtained on highly active, standard Au/TiO_2 catalysts [16]. Au catalysts supported on mesoporous titania and silica with Au particle sizes of 2–3 nm were described by Overbury et al. and evaluated with respect to their CO oxidation activity, but these results are hardly comparable to other data since the activity was characterized by light-off curves [21]. High reaction rates, comparable to those of good Au/TiO_2 catalysts with similar Au loading, were observed also by Pietron et al. for CO

Y. Denkwitz · R. J. Behm (✉)
Institute of Surface Chemistry and Catalysis, Ulm University, 89069 Ulm, Germany
e-mail: juergen.behm@uni-ulm.de

J. Geserick · N. Hüsing
Institute of Inorganic Chemistry I, Ulm University, 89069 Ulm, Germany

U. Hörmann · U. Kaiser
Central Facility of Electron Microscopy, Ulm University, 89069 Ulm, Germany

V. Plzak
Centre of Solar Energy and Hydrogen Research, Helmholtzstr. 8, 89081 Ulm, Germany

oxidation on different mesoporous Au/TiO_2 catalysts, [15]. In contrast, Schwarz et al. measured significantly lower CO oxidation activities on mesoporous Au/TiO_2 compared to a P25 based Au/TiO_2 catalyst [22]. These lower activities are most likely caused by the larger Au nanoparticles on their mesoporous Au catalyst compared to P25 based catalyst after similar conditioning treatment. Based on these different results, it is not really clear whether the use of mesoporous supports is a viable route for a substantial improvement of Au/TiO_2 catalyst, both with respect to their activity and, what has not been considered at all so far, with respect to their stability and deactivation.

In the present paper we report the first results on the CO oxidation characteristics of structurally well defined, mesoporous Au/TiO_2 catalysts, which were prepared by applying an established deposition-precipitation procedure for Au loading on mesoporous titania support materials. The mesoporous titania was prepared via two different routes, following either a procedure reported by Gedanken et al. [23] or that described in ref. [24]. The deposition-precipitation procedure was shown previously to reproducibly produce highly active catalysts with small Au nanoparticles ($\sim$3 nm after calcination) on P25 support material [11]. For comparison, we also include a standard Au/TiO_2 catalyst based on P25 support. Structural and chemical properties of the support material and the catalysts were characterized by various different methods including X-ray diffraction (XRD), transmission electron microscopy (TEM), and X-ray photoelectron spectroscopy (XPS). The activities and the deactivation behavior were evaluated by kinetic measurements under differential reaction conditions; mechanistic information, in particular on the deactivation process, was obtained from in-situ IR measurements employing diffuse reflectance IR spectroscopy (DRIFTS).

2 Experimental Set-up and Procedures

2.1 Preparation of the Mesoporous TiO_2 Support and of the Au Catalysts

The mesoporous TiO_2 support material was prepared via two different routes, denoted as (A) and (J). In the first one (A), following the procedure by Gedanken and coworkers, 0.89 g (3.3 mmol) octadecylamine (ODA) and 2.84 g (10 mmol) tetraisopropylorthotitanate (TIP, 98%) were dissolved in 10 mL ethanol and afterwards added to 40 mL water [23]. The resulting solution was irradiated with a high-intensity ultrasonic horn (Ti-horn, 20 kHz, 60 Wcm^{-2}), which leads to the precipitation of a white powder. This was filtrated, washed three times with water and dried at 60 °C over night. For complete removal of the surfactant, we employed two different procedures, either calcination in air for 6 h at 400 °C (A-1) or annealing at 350 °C under vacuum and subsequent calcination in air for 4 h at 400 °C (A-2) (see Table 1). The second route (J) involved the use of an ethylene glycol modified titanium precursor (bis(2-hydroxyethyl)titanate, EGMT) [24]. The EGMT was synthesized modifying a procedure described by Xia et al. [25]. Ethylene glycol (EG, 99.5%) and TIP (molar ratio 2:1) were dissolved in THF and refluxed for 5 h at 90 °C under argon. The evolving isopropyl alcohol and the THF were removed by distillation at 120 °C. EGMT was obtained as a white powder and dried under vacuum at 170 °C. For mesoporous TiO_2 synthesis, 0.55 g (0.81 mmol) polyethyleneoxide hexadecylether (Brij56, $M \sim 682$ g mol^{-1}) were dissolved in 100 mL dilute hydrochloric acid (pH 2). Subsequently, 4.53 g EGMT (26.95 mmol Ti) were added, and the solution was then treated in an ultrasonic bath for 5 h at 60 °C. The resulting suspension was aged in an oven at 60 °C for 24 h, and then centrifuged. The precipitate was washed with water three times and subsequently calcined at 400 °C (6 h) for complete surfactant removal (see Table 1).

The Au/TiO_2 catalysts were prepared by a deposition-precipitation procedure described in [26, 27]. In short, TiO_2 was suspended in water at 60 °C at a pH of 5–5.5, followed by addition of tetrachloroauric acid ($HAuCl_4 \cdot 4H_2O$), while maintaining a constant pH value by addition of Na_2CO_3 solution. After additional 30 min of stirring, the precipitate was cooled to room temperature, filtered, washed and dried overnight at room temperature under vacuum. The Au metal loading (Table 1) was determined by inductively coupled plasma atom emission spectroscopy (ICP-AES). Before the experiments, the samples were conditioned in-situ by calcination at 400 °C (30 min, 10% O_2/N_2). Based on ICP-AES and XPS results, the presence of Cl is below the detection limit of these methods.

2.2 Catalyst Characterization

The surface area and the pore diameter of the mesoporous support material and of the different catalysts were determined via N_2 porosimetry measurements (Autosorp MP1, Quantachrome). The resulting surface area was calculated using the Brunauer-Emmet-Teller (BET) relation in the p/p_0 range of 0.05 to 0.3. The pore size distribution was evaluated from the desorption branch of the isotherms, using the procedure developed by Barrett, Joyner and Halenda (BJH) [28]. XRD measurements were performed on a PANalytical MPD PRO instrument, using Cu K_α radiation (λ = 0.154 nm) to evaluate the titania structure and the titania particle sizes. The particle size and particle distribution of the Au nanoparticles (after calcination) were

Table 1 BET surface area, pore diameter, Au loading and TiO_2 crystallite size of Au/TiO_2 catalysts based on different (mesoporous) support materials

Catalyst	TiO_2 support synthesized with	Treatment of the support	Au loading/wt.%	TiO_2 crystallite size (XRD)/nm	BET surface area/$m^2\ g^{-1}$	Pore diameter (BJH)/nm	Pore volume/$cm^3\ g^{-1}$
Au/TiO_2 (P25)	–	–	3.1	21(anatase); 30 (rutile)	58	–	–
Au/TiO_2 (A-1)	ODA, TIP	6 h, air, 400 °C	2.8	12	63	3.6	0.15
Au/TiO_2 (A-2)	ODA, TiOP	20 h, vacuum, 350 °C 4 h, air, 400 °C,	3.5	9	99	3.7	0.43
Au/TiO_2 (J-1)	Brij56, EGMT	4 h, air, 400 °C	2.9	11	76	6.8	0.20
Au/TiO_2 (J-2)	Brij56, EGMT	4 h, air, 400 °C	3.5	9	110	5.1	0.20

derived from TEM images using a Philips CM 20 instrument (200 kV). Typically, several hundred particles (>600) were evaluated per sample for determining the size distribution of the Au particles. The relative surface concentrations and the oxidation states of Au, Ti, and O were determined by X-ray photoelectron spectroscopy (XPS) using monochromatized Al-K_α radiation (PHI 5800 ESCA system, Physical Electronic). The binding energies (BEs) were calibrated with respect to that of bulk Ti($2p_{3/2}$) (459.2 eV for Ti^{4+} [29]). Subtraction of a Shirley background and peak fitting were performed using a public domain XPS peak fit program (XPSPEAK4.1 by R Kwok).

2.3 Activity Measurements

The activity of the catalysts was determined in reaction measurements performed at atmospheric pressure in a quartz tube micro-reactor under differential reaction conditions, with typically 65–70 mg diluted catalyst powder. In order to limit the conversion to values between 5 and 20%, the catalyst was diluted with α-Al_2O_3, which is not active for CO oxidation. The experiments were carried out with a gas flow of 60 NmL min^{-1} in 1 kPa CO, 1 kPa O_2 and balance N_2 at 80 °C. Incoming and effluent gases were analyzed by on-line gas chromatography (Dani GC 86.10HT), using H_2 as carrier gas. High-purity reaction gases (CO: 4.7, O_2: 5.0 and N_2: 6.0; Westphalen) were used as delivered. The reaction rates were determined from the CO_2 partial pressure; for further information on the measurements see ref. [30]. Mass and heat transport problems are negligible, since the rates are below 10^{-5} mol s^{-1} cm^{-3} [31].

2.4 Infrared Measurements

In-situ IR measurements were performed by diffuse reflectance infrared fourier transform spectroscopy (DRIFTS) using a commercial in-situ reaction cell unit (Harricks, HV-DR2). The spectra were recorded in a Magna 560 spectrometer (Nicolet) equipped with a MCT narrow band detector. About 20 mg α-Al_2O_3 diluted catalyst (dilution 1:5) was used as a catalyst bed. Typically, 400 scans (acquisition time 3 min) were co-added for one spectrum. The intensities were evaluated in Kubelka-Munk units which are linearly related to the adsorbate concentration [32]. Background subtraction and normalization of the spectra was performed by subtracting spectra recorded in a flow of N_2 at the reaction temperature directly before starting CO oxidation. To remove changes in the reflectivity of the various catalysts, the spectra were scaled to similar intensity at 2,430 cm^{-1}, which did not interfere with any other signals and where the shape of the raw spectrum changed little during the measurements. The gas phase CO signal was removed by subtracting the spectral region of gas phase CO (2,140–2,240 cm^{-1}) of a spectrum recorded on pure α-Al_2O_3 in CO containing atmosphere.

3 Results and Discussion

3.1 Catalyst Characterization

After preparation along route (J), even the uncalcined 'as synthesized' TiO_2 was at least partially crystalline (Fig. 1, curve a), as evidenced by broad reflections in the XRD pattern at positions characteristic for anatase (crystallite size ~3 nm, Fig. 1, diffractogram a). Additional low intensity reflections at 44.58°(2θ) are related to stainless steel of the sample holder. Based on the N_2 sorption measurements, the BET surface area of the dried, but uncalcined sample is about 450 $m^2\ g^{-1}$. Calcination of this sample at 400 °C for 4 h decreases the surface area and leads to further crystallization, resulting in pure anatase nanocrystals (Fig. 1, curve b). Pores of 5–7 nm in diameter are attributed to aggregation of the nanocrystals. In contrast, for the TiO_2 sample prepared along route (A), we

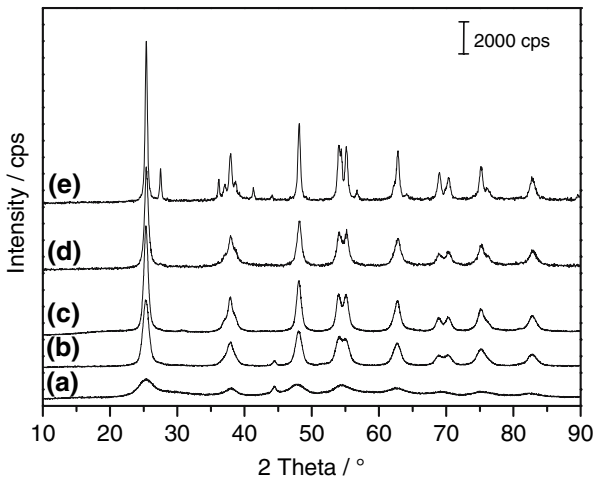

Fig. 1 XRD pattern of the (**a**) as-synthesized support synthesized with EGMT and Brij56, (**b**) support from (**a**) after calcination for 4 h at 400 °C, (**c**) Au/TiO_2 (J-type), (**d**) Au/TiO_2 (A-type) and (**e**) Au/TiO_2 based on commercial TiO_2 (P25)

obtained an amorphous framework, similar to results by Wang et al. [23]. During calcination, crystallization sets in, leading to a pure anatase modification, and pores of about 3.5 nm develop, as determined by N_2 sorption. Also the pore diameter resembles results by Wang et al.

The diffractograms (c) and (d) in Fig. 1 show that Au deposition on the mesoporous support materials does not affect the crystalline structure of the support; the resulting mesoporous Au/TiO_2 catalysts exhibit only the characteristic anatase reflections. For comparison, we also include a diffractogram recorded on a catalyst prepared from commercial TiO_2 (P25, Degussa AG). As expected, this reveals additional reflections of the rutile modification (Fig. 1, curve e). Based on the width of the reflections, the crystallite sizes of the mesoporous supports are rather small and about similar ($\sim$10 nm) for both types (see Table 1), while for Au/TiO_2(P25) they are larger (21 and 30 nm for rutile and anatase, respectively). The reflections of the Au particles are not visible because of the very small Au particle sizes prior to calcination (1.3 nm [33]). For the mesoporous Au/TiO_2 catalysts, we obtained BET surface areas of 70 and 110 $m^2\ g^{-1}$ and pore diameters of 5 and 7 nm, respectively, for the J-type catalysts upon identical support treatment. For the Au/TiO_2 (A) catalysts, both samples showed the same pore diameter ($\sim$3.6 nm), while surface areas of 63 and 99 $m^2\ g^{-1}$ were obtained (Table 1). In this case, the difference may also be related to the different post-treatment of the oxide (see Table 1).

TEM imaging showed that after 30 min calcination (10% O_2, N_2) at 400 °C the Au/TiO_2(P25) catalyst consists of TiO_2 crystallites with diameters between 5 and 60 nm, in agreement with the mean diameters obtained from XRD, and that the particles are partly facetted (Fig. 2e). The mesoporous samples show smaller TiO_2 crystallites whose size varies between 5 and typically 15 or 30 nm for the A-type and J-type catalyst, respectively, comparable to the XRD results. These crystallites are connected via grain boundaries, forming an open framework with pores between the crystallites. For the J-type samples, the framework structures form irregular, large aggregates with no specific morphology (Fig. 2a, b), while for the A-type Au/TiO_2 samples spherical particles are obtained, whose sizes range from 20 to 300 nm in diameter (Fig. 2c, d). Most likely, this difference compared to the J-type samples is due to the ultrasonication process employed during synthesis of the A-type samples. Based on the XRD results, the crystallites consist of anatase, and these crystallites are more densely packed in the A-type than in the J-type Au/TiO_2 sample, which results in a smaller pore diameter (intra-particle pores) as already concluded from the BJH measurements (Table 1).

The TEM images furthermore revealed a homogeneous distribution of the Au nanoparticles in framework structures, i.e., in the mesopores, and on the outer surface (Fig. 2). The Au nanoparticle size distribution of the various catalyst resulted in mean particle sizes of 2.4–2.9 ± 0.7 nm, independent of the support material (Fig. 2f–h, Table 2). Hence, further Au particle growth would not be limited by the pore structure of the support. The resulting Au particle sizes are in good agreement with previous results for calcined Au catalysts based on anatase or P25 [11, 26]. In contrast, Schwartz et al. reported a much more pronounced Au particle growth upon calcination. They obtained a mean particle size of $\sim$10 nm for their mesoporous Au/TiO_2 catalysts upon calcination 300 °C (150 °C annealing in H_2: 3 nm), compared to the $\sim$3 nm in our case (calcination at 400 °C). These results are clearly not compatible with our present findings. They furthermore reported that the Au particle growth depends on the modification of titania, with an increasing tendency for Au sintering in the order brookite < anatase < P25 $\approx$ rutile < mesoporous TiO_2 [22]. An effect of the support modification on the stability of the Au nanoparticles and thus also on their CO oxidation activity was reported also by Yan et al. [34], who observed significantly less Au sintering upon calcination of a brookite based than for an anatase based Au/TiO_2 catalyst.

The surface composition of the different catalysts after calcination at 400 °C (30 min 10% O_2/N_2) was characterized by XPS (see Fig. 3 and Table 2). Survey spectra (not shown) show peaks related to Ti, O and Au as well as some C. Detail spectra recorded in the Ti(2p) (not shown) and Au(4f) regions reveal the following trends: The Ti(2p) spectra show completely oxidized Ti^{4+} species (459.2 eV [29]). For all catalysts, Au is present mainly as metallic Au^0, (84.0 ± 0.1 eV) [29] with Au^{3+} (85.9 ± 0.1 eV)

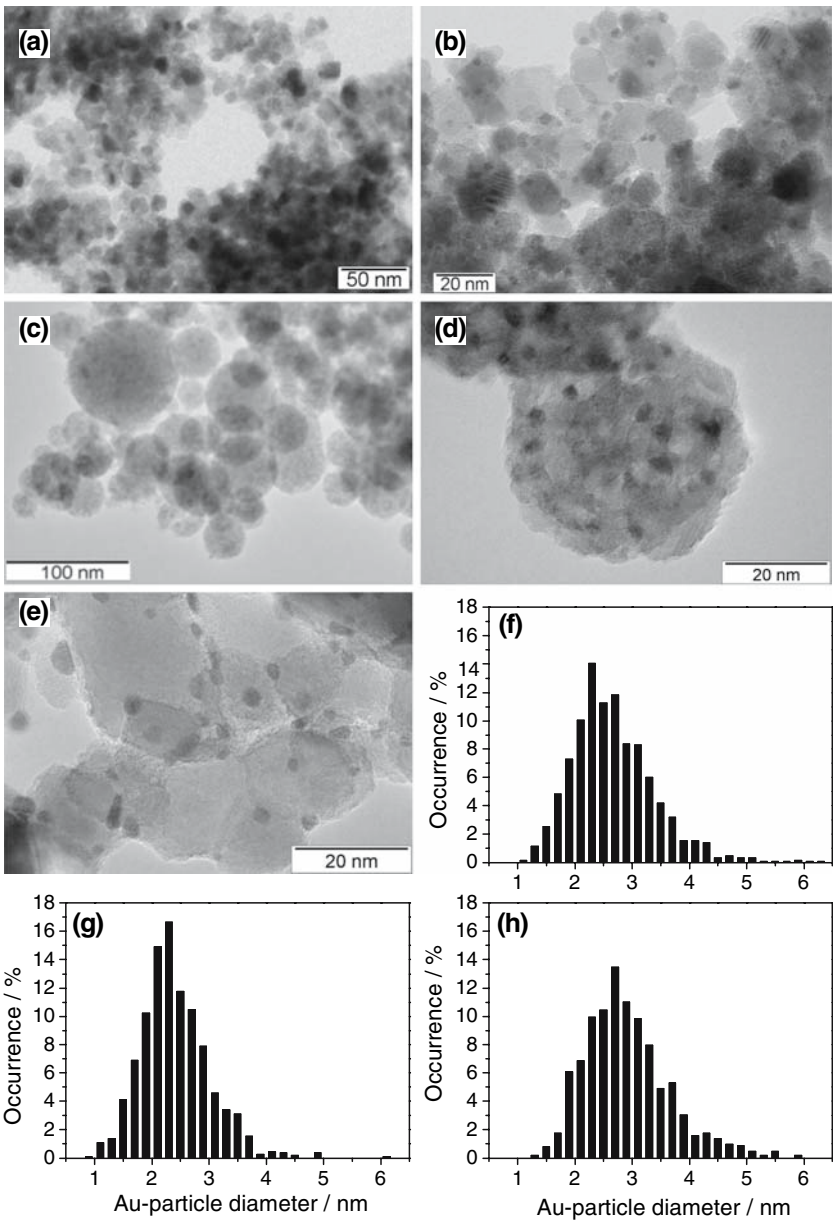

Fig. 2 Larger scale (**a**, **c**) and high resolution (**b**, **d**, **e**) TEM images and Au particle size distribution (**f**–**h**) of J-type mesoporous TiO_2 (**a**), a J-type mesoporous catalysts (**b**, **f**), an A-type mesoporous catalyst (**c**, **d**, **g**) and of the P25 based Au/TiO_2 catalyst (**e**, **h**) after conditioning at 400 °C (30 min, 10% O_2/N_2)

Table 2 Mean Au particle size, Au(4f):Ti(2p) intensity ratio, absolute and relative activity for CO oxidation as well as activation energy for CO oxidation of/on various Au/TiO_2 catalysts after calcination in 10% O_2/N_2 at 400 °C

Catalyst	Au-particle size/nm	Au(4f): Ti(2p) ratio	Initial/finial activity (TOF)/s^{-1}	Activity after 1,000 min reaction/%	Activation energy/kJ mol^{-1}
Au/TiO_2(P25)	2.9 ± 0.7	0.13	1.6/1.2	75	33 ± 3
Au/TiO_2 (A-1)	2.4 ± 0.6	0.12	1.2/1.0	83	36 ± 4
Au/TiO_2 (A-2)	2.9 ± 0.7	0.08	1.6/1.3	80	36 ± 4
Au/TiO_2 (J-1)	2.7 ± 0.7	0.09	2.2/1.9	88	31 ± 3
Au/TiO_2 (J-2)	2.8 ± 0.7	0.05	2.0/1.7	86	28 ± 3

[35, 36] contributions of ~2% and ~4% for Au/TiO_2 based on the P25 and on the mesoporous TiO_2 support, respectively (Fig. 3). In total, there are no significant differences between the P25 based catalyst and the mesoporous catalysts as far as the surface composition is concerned. The $I_{Au(4f)}/I_{Ti(2p)}$ ratio decreases slightly with

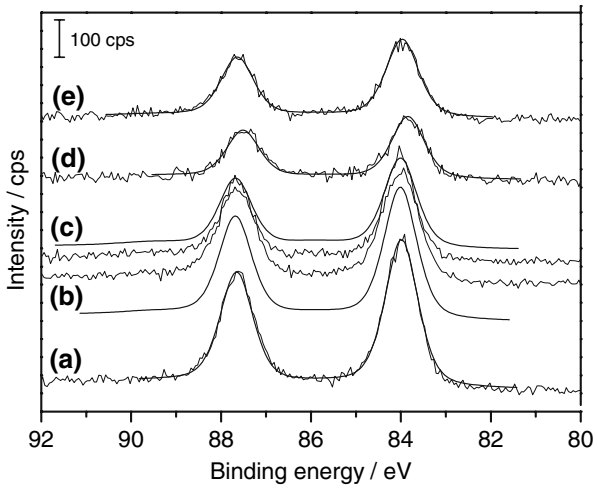

Fig. 3 XP Spectra of the Au(4f) region of Au/TiO_2 (**a**) P25, (**b**) A-1, (**c**) J-1, (**d**) A-2 and (**e**) J-2 after conditioning (10% O_2/N_2 at 400 °C)

increasing surface area at comparable Au loading (Table 2), reflecting the increasing amount of Au nanoparticles deposited on the inner surface, in the pores.

3.2 CO Oxidation Activity

The activity and deactivation of the different Au/TiO_2 catalysts with time during CO oxidation in a standard reaction mixture (1 kPa CO, 1 kPa O_2, rest N_2) at 80 °C are illustrated in Fig. 4. The top panel depicts the evolution of the activity under these reaction conditions, described by the turn-over frequencies (TOFs). TOF numbers were calculated from the mass specific rates using the mean Au particle size (Table 2). The bottom panel shows the deactivation on a relative scale, normalized to an initial activity of 100%. The catalytic properties reveal a clear influence of the different support materials, both for the activity and for the deactivation behavior. The highest activity is found for Au/TiO_2(J-1) (Fig. 4, empty squares) followed by Au/TiO_2(J-2) (filled squares). The (initial) reaction rate of the P25 based catalyst (Fig. 4, empty circles) is comparable with that of 'good' Au/TiO_2 catalysts reported in previous studies [3, 12, 13, 26, 37]. The activity of the catalyst Au/TiO_2(A-2) (Fig. 4, filled triangles) is comparable to that of the Au/TiO_2(P25) sample, the lowest value is obtained on the Au/TiO_2 (A-1) sample (Fig. 4, empty triangles). The main differences between the mesoporous catalysts and the P25 based Au/TiO_2 catalyst are the different support morphologies, including (i) the pore structure and (ii) crystallite and particle size, and iii) surface areas, and (iv) the modification of the TiO_2 support (P25: 75% anatase, 25% rutile; mesoporous TiO_2: pure anatase). Considering this and the comparable chemical state of the catalysts, with exclusively Ti^{4+} and metallic Au^0 species, as well as the comparable Au particle sizes of the catalysts (see above), the activity differences between the mesoporous catalysts and the P25 based catalyst must be due to the difference in pore structure or to the additional rutile component in the commercial catalyst. Since the activity difference between J-type catalyst and P25 based catalyst is more than the rutile contribution to the latter catalyst (25%), the pore structure must have a beneficial effect on the activity of the J-type catalyst. Similarly, the lower activity of the A-type catalyst, which equally consists of anatase crystallites, also points to effects of the pore structure (see below).

Comparison with previous reports on CO oxidation over mesoporous Au/TiO_2 catalysts [15, 21, 22] leads to the following results: The high Au mass normalized activity reported by Pietron et al. [21] is comparable to our observations. They explained the high activity by the shorter diffusion pathways of CO_{ad} to the interface region between Au nanoparticles and TiO_2 due to the fact that the Au nanoparticles (mean diameter 5.5 nm) were contacted at more than one position by the TiO_2 anatase substrate (mean pore size 10–12 nm) [15]. In contrast, Schwarz et al.

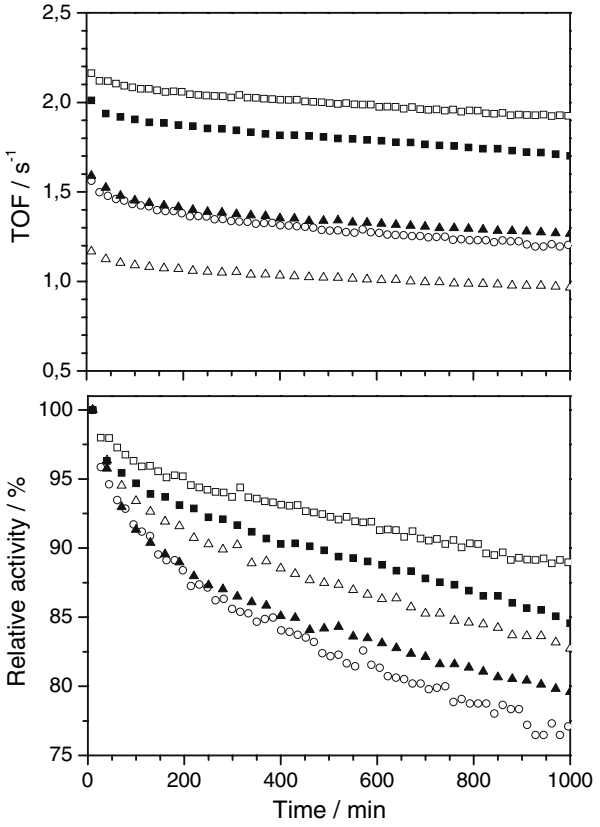

Fig. 4 Evolution of the mass-specific CO oxidation rate (top) and the relative conversion (bottom) on various Au/TiO_2 catalysts: (□) J-1, (■) J-2, (△) A-1, (▲) A-2, and (○) P25, during 1,000 min reaction at 80 °C in standard reaction mixture (1% CO, 1% O_2, balance N_2)

reported a lower activity of their mesoporous Au/TiO_2 catalysts compared to Au catalysts based on nonporous TiO_2 (brookite, anatase, rutile) [22]. Most likely, this does not reflect a direct catalytic substrate effect, but results from the much larger Au particle size in the mesoporous catalyst ($\sim$10 nm, see above).

Considering the different aspects, the higher activity of the mesoporous Au/TiO_2 catalysts is tentatively attributed to the higher interface area of Au nanoparticles in the pores with more than one contact to the support, which increases the number of adlineation sites, i.e., accessible sites at the interface between Au nanoparticles and titania support.

The long-term stability of the catalysts is plotted in the bottom panel in Fig. 4, normalized to an initial activity of 100% for each catalyst. Clearly, the stability of the mesoporous catalysts is better than that of Au/TiO_2(P25), with a deactivation by 12–15% for the J-type catalysts and by 17–20% for the A-type catalysts after 1,000 min reaction. In contrast, the activity of Au/TiO_2(P25) decreased by 25% of the initial value, which is significantly more than the deactivation of the mesoporous catalysts. Following previous studies, where sintering of the Au nanoparticles was found to be negligible during CO oxidation under similar reaction conditions [12, 26], Au particle growth is ruled out as origin for the deactivation. Therefore, stabilization of the Au nanoparticles in the TiO_2 mesopores preventing Au particle growth cannot be the reason for the lower deactivation of the mesoporous catalysts. Schumacher et al. in fact reported a higher deactivation tendency of P25 supported catalysts compared to Au catalysts supported on pure, non-mesoporous anatase and related this to the additional presence of rutile [11, 26]. It is well known from studies on P25 based catalysts that deactivation is accompanied by a significant growth in surface carbonate and decrease in CO_{ad} steady-state coverage under reaction conditions and the increasing covering of the oxide support by surface carbonates was made responsible for the deactivation [26, 33, 38]. Consequences for the present mesoporous catalysts will be discussed in more detail in the next section, together with the IR data.

From measurements under similar reaction conditions, performed in the temperature range of 50–110 °C and after an initial deactivation run of 1,000 min, we determined the activation energies of the CO oxidation reaction on the different Au/TiO_2 catalysts. They are listed in Table 2. The value obtained on the P25 based catalyst, 33 ± 3 kJ mol^{-1}, agrees well with previous results measured on catalysts with comparable characteristics and under comparable reaction conditions [4, 13, 37, 39]. On the mesoporous catalysts, the activation energies are slightly higher for the A-type catalyst (36 ± 4 kJ mol^{-1}), and slightly lower for the J-type catalysts (30 ± 3 kJ mol^{-1}). Considering the error in the experiments, however, the differences are too small to regard them as significant. The close similarity of the activation barrier points to a similar rate limiting step for the different catalysts, which is at most slightly modified by the different support modifications.

3.3 Infrared Investigations

The surface species adsorbed under reaction conditions and their accumulation with time, during reaction, was followed by in-situ DRIFTS measurements performed with similar reaction parameters as used for the kinetic studies (1 kPa CO, 1 kPa O_2 and N_2 at 80 °C). Different from the latter experiments, the CO conversion was no longer small, i.e., the reaction was not performed under differential reaction conditions, due to the limitations in catalyst dilution to have enough IR signal intensity. Nevertheless, since the IR data are measured on the topmost catalyst layer in the reaction cell, which is exposed to the incoming gas stream, we believe that the results can at least qualitatively be correlated with the results of the kinetic measurements [33].

Spectra recorded at the beginning of the reaction and after 1000 min reaction are shown in Fig. 5a and b, respectively. All catalysts exhibit the same characteristic features, with bands at 2,118–2,124 cm^{-1} representative for CO adsorbed on metallic Au, at 2,339 and 2,361 cm^{-1} characteristic for gaseous CO_2, and a set of vibrational bands in the range between 1,350 and 1,560 cm^{-1}, which are commonly attributed to C=O and O–C–O vibrations of carbonates, carboxylates, bicarbonates and formates (see below). Based on absence of C–H signals in the range typical of formate species (2,970–2,950 and 2,880–2,885 cm^{-1}) [40], formate formation is negligible. (The small signals at 2,914 and 2,848 cm^{-1} are an artifact, due to contributions from the mirrors). Isolated OH groups, reflected by peaks at 3,724 and 3,675 cm^{-1} [41–43], are removed in the very beginning of the reaction, as evidenced by the negative peaks in Fig. 5a [42, 43]. Finally, the intensity of the water signals at $\sim$1,630 cm^{-1} and 2,500–3,300 cm^{-1} is very small and does not change significantly during the reaction. In the absence of formate and bicarbonate species—the latter species were found to be instable on Au/TiO_2 under present reaction conditions [8]. Bands in the range between 1,350 and 1,560 cm^{-1} can be related to the C=O stretch vibration ν(C=O) of bidentate carbonates ($\sim$1,527 cm^{-1}), to the symmetric stretch vibration ν_s(COO) of monodentate carbonates (1,356 cm^{-1}) and the asymmetric stretch vibration ν_{as}(COO) of monodentate carbonates (in the range 1,430–1,530 cm^{-1}), and to the asymmetric and symmetric stretch vibration of carboxylates (1,560–1,620 cm^{-1} and 1,400–1,420 cm^{-1}), respectively [9, 44, 45]. These signals

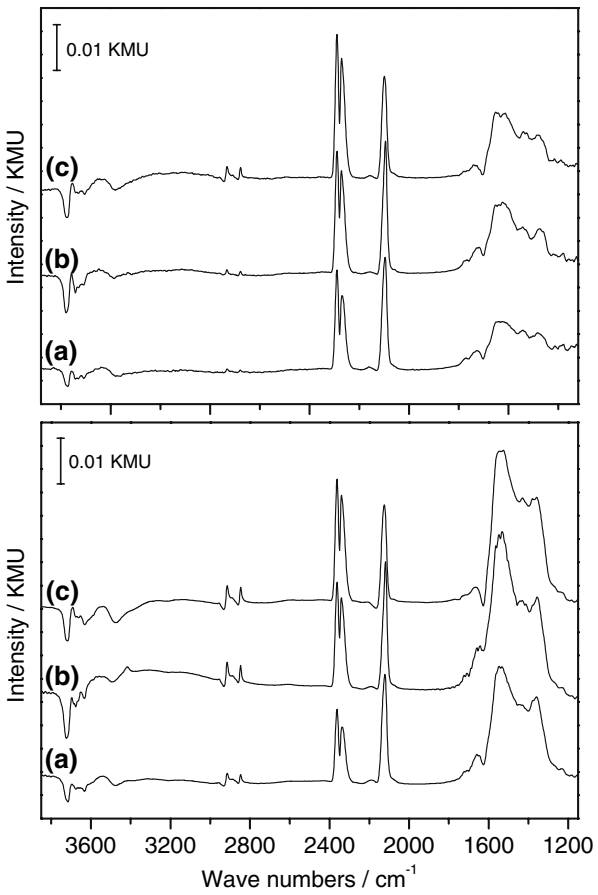

Fig. 5 In-situ DRIFT spectra recorded during CO oxidation on different Au/TiO_2 catalysts (A-type: spectrum (**a**), P25 based: spectrum (**b**), J-type: spectrum (**c**) in a standard reaction mixture (1% CO, 1% O_2, balance N_2) at 80 °C at the beginning (1 min) of the reaction (top panel) and after 1,000 min reaction (bottom panel). The spectra are normalized to a similar reflectivity of the catalysts (see experimental)

overlap considerably, rendering a quantitative evaluation of the different signals almost impossible. Unique and clearly identifiable features are the bands at $\sim$1,420 cm^{-1} (most likely carboxylates [33]) and 1,356 cm^{-1} (monodentate carbonate). The broad plateau between 1,527 and 1,564 cm^{-1} observed after 1,000 min reaction developed from at least two closely neighbored bands at 1,527 and 1,564 cm^{-1} (see spectra in the top panel). Considering that in a recent study on a P25 based Au/TiO_2 catalyst a band at 1,406 cm^{-1} related to carboxylates was found to be much more intense upon reaction at 30 °C than at 80 °C [33], carboxylate species are expected to be significantly less stable than the monodentate carbonate species and to represent a small contribution to the adlayer at 80 °C, with monodentate carbonate species being dominant. The frequencies of the different surface species are virtually identical on the different various catalysts, with the largest difference observed for the CO_{ad} band at 2,118, 2,120 and 2,124 cm^{-1} for the P25, A-type and J-type catalyst, respectively.

The temporal evolution of the different peak intensities during reaction is illustrated in Fig. 6, where the integrated intensities of the CO_2 related signal (Fig. 6a), of the CO_{ad} related band (Fig. 6b), and of the carbonate/carboxylate related band (Fig. 6c) at 2,339–2,361 cm^{-1}, 2,112–2,120 cm^{-1}, and 1,359/1,420/1,527–1,564 cm^{-1}, respectively, are plotted as a function of time. The carbonate/carboxylate related band intensity was determined by integrating the intensity between 1,270 and 1,750 cm^{-1} which can be justified since under present reaction conditions other species with signals in this wavenumber range such as water ($\sim$1,630 cm^{-1}) or formates (see above) are essentially absent. As described in the experimental section, the intensities are scaled to similar reflectivity on the different catalysts.

We find an almost similar decay of the CO_{ad} and CO_2 related intensities, after passing through an initial maximum, and a steady increase of the carbonate related intensity with time, for all catalysts. In analogy to the activities determined in the kinetic measurements (Fig. 3), the CO_2 related intensity is significantly higher on the J-type mesoporous Au/TiO_2 catalyst than on the Au/TiO_2(P25) sample, and is lowest on the A-type Au/TiO_2 catalyst. After 1000 min reaction, the CO_2 intensity has decreased to 87% for the J-type and P25 based Au/TiO_2 catalysts, while on the A-type Au/TiO_2 catalyst it decreased to 74% of the initial intensity, after 10 min reaction. (The intensities after 10 min were used as standard to have a similar normalization point as in the kinetic measurements, where the first GC measurement was performed after 10 min reaction.)

The formation of an initial maximum of the CO_2 signal intensity after 2–3 min reaction instead of a steep increase and a subsequent slow decay can be explained by the finite time required to reach steady-state conditions in the gas phase of the DRIFTS cell (note that the final intensity of the CO gas phase signal is reached $\sim$70 s after switching from N_2 to the reaction mixture) and in the adlayer composition. For the latter, equilibration takes even longer, as evidenced by the ongoing increase of the CO_{ad} intensity, where the maximum is reached only after 40–100 min.

The carbonate signals show a strong intensity increase within the first 15 min of the reaction, which then levels off to a slower and almost linear increase. The correlation between carbonate intensity growth and CO_{ad} intensity/CO_2 formation rate decay with time resembles our results for CO oxidation on conditioned and non-conditioned P25 based Au/TiO_2 catalysts [8, 26, 33]. The order of the final carbonate intensity, I_{carb}(J-type) $\geq$ I_{carb}(P25) > I_{carb} (A-type) supports our previous proposal that the deactivation of the Au/TiO_2 catalysts is mainly caused by the

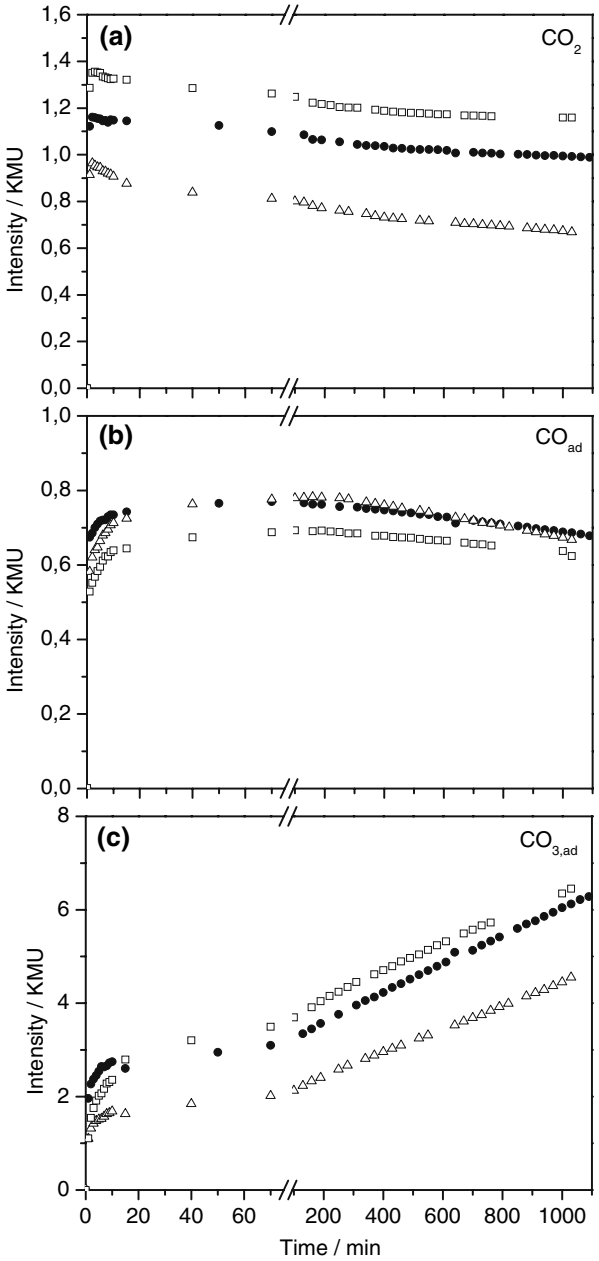

Fig. 6 Intensity of the in-situ DRIFTS signals characteristic for CO_2 (**a**), for CO_{ad} (**b**) and for the carbonate region (**c**) as a function of time during CO oxidation on the different Au/TiO_2 catalysts (A-type: △, P25 based: ●, J-type: □) at 80 °C in a standard reaction atmosphere (1% CO, 1% O_2, balance N_2). The intensities are normalized to a constant similar reflectivity of the catalyst (see experimental)

formation of a reaction inhibiting adlayer of stable monodentate carbonates [26]. Since based on their vibrational characteristics the carbonates are located on the oxide substrate, the influence on the CO_2 formation must be indirect, e.g., by blocking the reverse spill-over of CO_{ad} from the oxide substrate to Au nanoparticles and to the active sites, which would also explain the decreasing amount of CO adsorbed on the Au nanoparticles with time. Furthermore, the carbonate species could affect the reactivity by blocking active sites at the perimeter of the Au nanoparticles ('adlineation sites') (see also [33]). Since the mesoporous catalysts exhibit a higher oxide surface area than the P25 based catalyst, the carbonate adlayer is, for similar amounts of surface carbonates, less dense on them, which explains in a simple way the lower tendency for carbonate induced deactivation and hence higher stability of the mesoporous Au/TiO_2 catalysts compared to the P25 based catalyst under present reaction conditions.

4 Summary

We have investigated the activity and stability of new mesoporous Au/TiO_2 catalysts in the CO oxidation reaction as well as the molecular mechanisms underlying the deactivation by kinetic measurements under differential reaction conditions and by in-situ DRITFTS. The catalysts were prepared by deposition-precipitation of Au on the mesoporous titania support material and subsequent calcination at 400 °C. Mesoporous titania was synthesized via two different routes, involving different Ti precursors and surfactants (A-type: TIP/ODA, J-type: EGMT/Brij56), respectively. Calcination at 400 °C results in titania supports made up from small anatase crystallites (crystallite size ~10 nm), forming either open frameworks with pores of 6.8 nm diameter (J-type) or spherical particles (diameter 20–200 nm) with pores of 3.6 nm diameter (A-type). The resulting Au/TiO_2 catalysts (Au particle size ~3 nm) showed a high activity for CO oxidation, comparable to (A-type) or higher than (J-type) that of highly active Au/TiO_2 catalysts based on commercial TiO_2 (P25). Both mesoporous Au/TiO_2 catalysts show a lower tendency for deactivation than the standard P25 based catalyst. In-situ IR measurements revealed a clear correlation between increasing carbonate coverage and decreasing CO_{ad} intensity and CO_2 formation rate, indicating that the formation of a reaction inhibiting carbonate adlayer is the main origin for deactivation, e.g., by decreasing the extent of reverse spill-over of CO_{ad} or by blocking active sites at the interface between Au nanoparticles and support ('adlineation sites'). The higher stability of the mesoporous catalyst was explained by their higher surface area compared to the P25 based catalyst, leading to a lower density of the carbonate adlayer and hence lower effect on the reactivity. The higher activity was tentatively attributed to the higher interface area of Au nanoparticles in the pores with more than one contact to the support.

Acknowledgments This work was supported by the Deutsche Forschungsgemeinschaft within the Priority Programme (SPP) 1181 'Nanomat' (Be 1201/13-1, Hu 1427 1/1 and Ka-1295/5-1).

References

1. Bond GC, Thompson DT (1999) Catal Rev Sci Eng 41:319
2. Mul G, Zwijnenburg A, van der Linden B, Makkee M, Moulijn JA (2001) J Catal 201:128
3. Haruta M (2004) Gold Bull 37:27
4. Haruta M (1997) Catal Surv Jpn 1:61
5. Boccuzzi F, Chiorino A (2000) J Phys Chem B 104:5414
6. Bond GC, Thompson DT (2000) Gold Bull 33:41
7. Haruta M (2002) CATECH 6:102
8. Schumacher B, Denkwitz Y, Plzak V, Kinne M, Behm RJ (2004) J Catal 224:449
9. Grunwaldt J-D, Maciejewski M, Becker OS, Fabrizioli P, Baiker A (1999) J Catal 186:458
10. M Daté, Ichihashi Y, Chiorino A, Boccuzzi F, Haruta M (2002) Catal Today 72:89
11. Schumacher B, Plzak V, Cai J, Behm RJ (2004) Catal Lett 101:215
12. Zanella R, Giorgio S, Shin C-H, Henry CR, Louis C (2004) J Catal 222:357
13. Moreau F, Bond GC (2006) Appl Catal A 302:110
14. Karpenko A, Leppelt R, Plzak V, Cai J, Chuvilin A, Schumacher B, Kaiser U, Behm RJ (2007) Topics Catal 44:183
15. Pietron JJ, Stroud RM, Rolison DR (2002) Nano Lett 2:545
16. Tai Y, Murakami J, Tajiri K, Ohashi F, Daté M, Tsubota S (2005) Appl Catal A 268:183
17. Liu J-H, Chi Y-S, Lin H-P, Mou C-Y, Wan B-Z (2004) Catal Today 93–95:141
18. Chiang C-W, Wang A, Wan B-Z, Mou C-Y (2005) J Phys Chem B 109:18042
19. Venezia AM, Liotta FL, Pantaleo G, Beck A, Horvath A, Geszti O, Kocsonya A, Guczi L (2006) Appl Catal A 310:114
20. Chiang C-W, Wang A, Mou C-Y (2007) Catal Today 117:220
21. Overbury SH, Ortiz-Soto L, Zhu H, Lee B, Amiridis MD, Dai S (2004) Catal Lett 95:99
22. Schwartz V, Mullins DR, Yan W, Chen B, Dai S, Overbury SH (2004) J Phys Chem B 108:15782
23. Wang Y, Tang X, Yin L, Huang WP, Hacohen YR, Gedanken A (2000) Adv Mater 12:1183
24. Geserick J, Hüsing N, Rosmanith R, Landfester K, Weiss CK, Denkwitz Y, Behm RJ, Hörmann U, Kaiser U (2007)
25. Xia Y, Xuchuan J, Herricks T (2003) Adv Mater 15:1205
26. Schumacher B, Plzak V, Kinne M, Behm RJ (2003) Catal Lett 89:109
27. Plzak V, Garche J, Behm RJ (2003) Eur Fuel Cell News 10:8
28. Barrett EP, Joyner LG, Halenda PP (1951) J Am Chem Soc 73:373
29. Moulder JF, Stickle WF, Sobol PE, Bomben KD (1992) Handbook of X-ray photoelectron spectroscopy. Perkin Elmer Corp., Eden Prairie/USA
30. Kahlich MJ, Gasteiger HA, Behm RJ (1997) J Catal 171:93
31. Weisz PB (1992) Chem Engin Progr Symp Ser 55:29
32. Hamadeh IM, Griffiths PR (1987) Appl Spec 41:682
33. Denkwitz Y, Zhao Z, Hörmann U, Kaiser U, Plzak V, Behm RJ (2007)
34. Yan W, Chen B, Mahurin SM, Dai S, Overbury SH (2004) Chem Commun 1918
35. Dickinson T, Povey AF, Sherwood PMA (1974) J Chem Soc Faraday Trans 71:298
36. Holm R, Storp S (1976) Appl Phys 9:217
37. Rossignol C, Arrii S, Morfin F, Piccolo L, Caps V, Rousset J-L (2005) J Catal 230:476
38. Konova P, Naydenov A, Venkov Cv, Mehandjiev D, Andreeva D, Tabakova T (2004) J Mol Catal A 213:235
39. Okumura M, Nakamura S, Tsubota S, Nakamura T, Azuma M, Haruta M (1998) Catal Lett 51:53
40. Busca G, Lamotte J, Lavalley J-C, Lorenzelli V (1987) J Am Chem Soc 109:5197
41. Zaki MI, Knözinger H (2003) Mat Chem Phys 17:201
42. Kim KS, Barteau MA (1988) Langmuir 4:945
43. Finnie KS, Cassidy DJ, Bartlett JR, Woolfrey JL (2001) Langmuir 17:816
44. Davydov AA (1984) Infrared spectroscopy of adsorbed species on the surface of transition metal oxides. John Wiley & Sons Ltd., Chichester, UK
45. Bollinger MA, Vannice MA (1996) Appl Catal B 8:417